## FIGURE S1

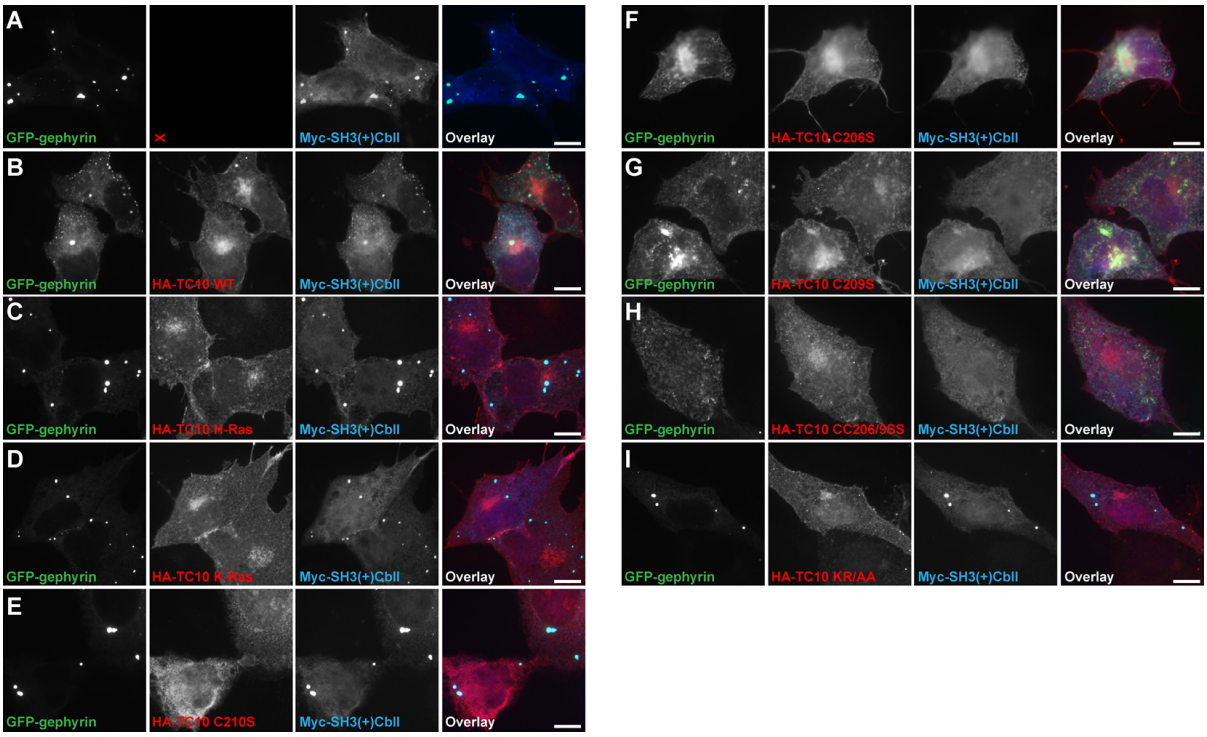


**Fig. S1. Effects of the different HA-TC10 mutants on the Cb-mediated clustering of gephyrin in COS7 cells.** Representative images of COS7 cells cotransfected with GFP-gephyrin and Myc-SH3(+)CbII in the presence or absence of HA-TC10 WT or mutant proteins, as indicated, and used in the quantifications shown in Fig. 1B. Scale bars: 10 μm.

**FIGURE S2**

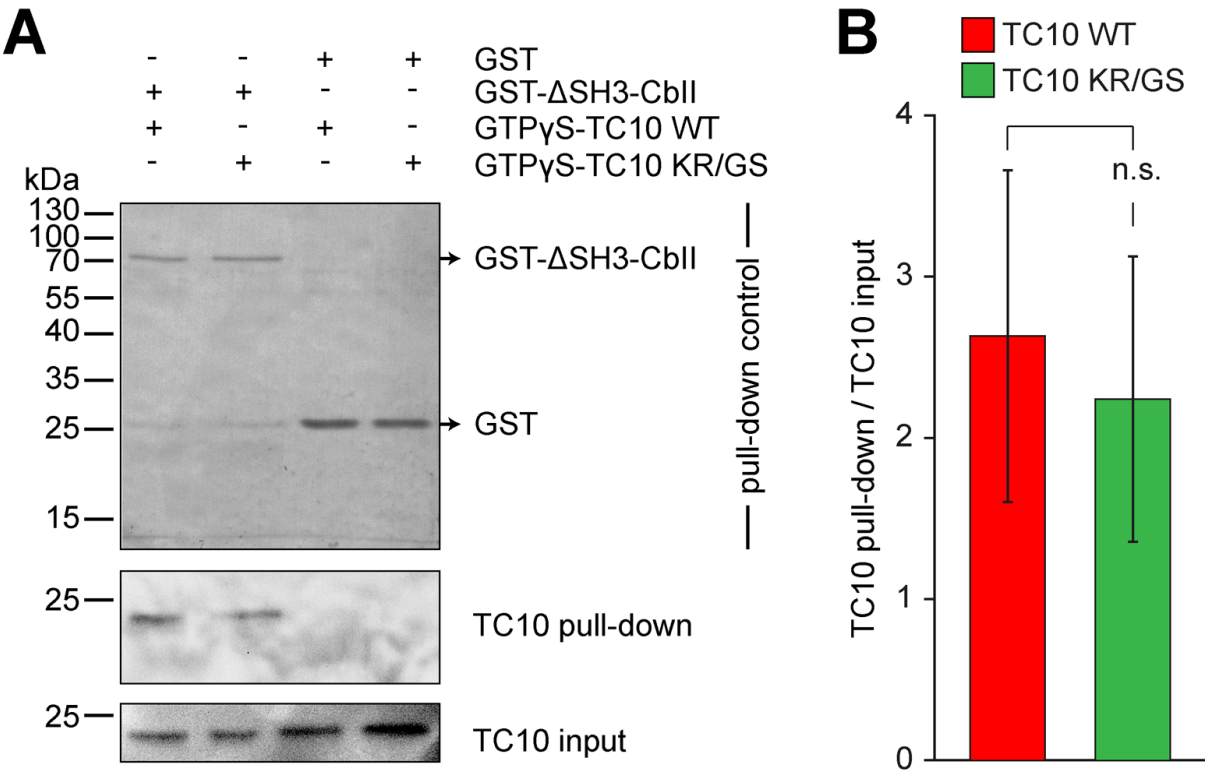


**Fig. S2. The TC10 KR/GS mutant retains its binding to Cb.** (A) Purified and GTPγS-loaded TC10 WT or the TC10 KR/GS mutant were incubated with the indicated recombinant proteins bound to glutathione-Sepharose beads. Center panel: Bound TC10 (WT or KR/GS) was detected by Western blotting using a TC10-specific polyclonal antibody (TC10 107573, 1:1000; Abcam). Note that both, TC10 WT and the TC10 KR/GS mutant bound to GST-ΔSH3-CbII but not to GST alone. Top pannel: MemCode stainings of the same membrane prior to TC10 immunoblotting indicating the amounts of GST-tagged bait proteins used in the actual reaction mixture. Bottom panel: To ensure that similar amounts of TC10 were included in all reaction mixtures, 2% of the premixed reactions were stored and subsequently subjected to anti-TC10 Western blotting using the TC10 107573 antibody. (B) Quantifications (ratios of relative band intensities of pulled down TC10 / total TC10) of TC10 WT or the KR/GS mutant bound to GST-ΔSH3-CbII. Data represent means ± SEM (n.s., not significant; unpaired, two-tailed Student's t-test) of n=3 independent experiments.

**FIGURE S3**

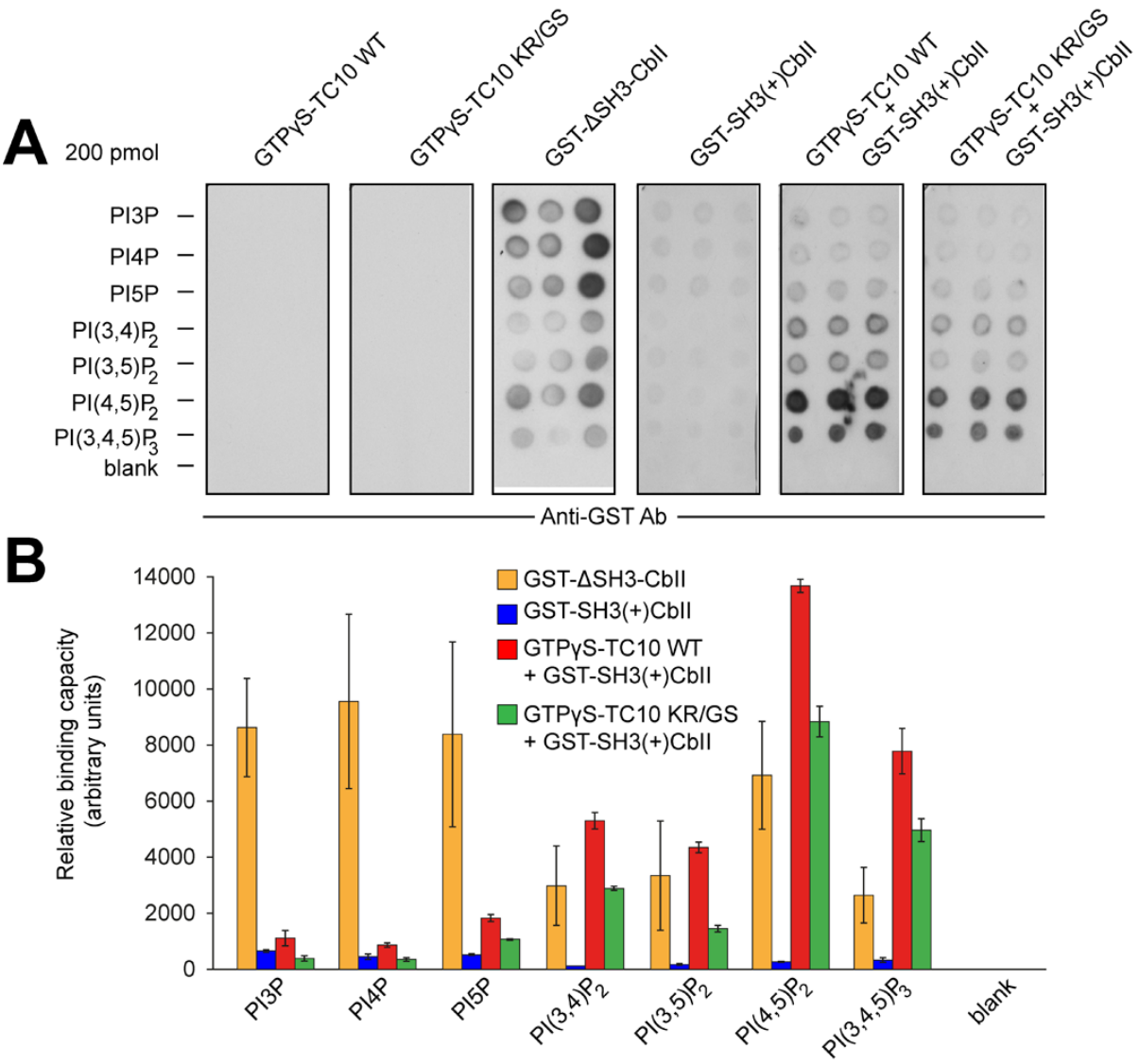


**Fig. S3. Both TC10 WT and TC10 KR/GS specifically regulate the binding of Cb to certain phosphoinositides.** (A) Protein-lipid overlay assays using GTPγS-TC10 WT, GTPγS-TC10 KR/GS and GST-ΔSH3-CblI, or GST-SH3(+)CblI, either alone or in a 1:1 ratio (0.5 µg/ml of each protein), as indicated on the top of the membranes. 200 pmol of the different phosphoinositides (Echelon, PInPs-diC16) were spotted onto the Hybond-C-extra membranes (GE Healthcare), as indicated. Interactions of Cb with the different phosphoinositides were detected by incubating the membranes with a goat anti-GST-HRP conjugate (GE Healthcare). As shown previously (Ludolphs et al., 2016), ΔSH3-CblI binds to a broad range of phosphoinositides, including monophosphorylated (PI3P, PI4P, PI5P) and diphosphorylated [$PI(4,5)P_2$] ones. However, in contrast to Ludolphs et al., 2016, an elevated interaction of ΔSH3-CblI with $PI(3,4,5)P_3$ was not observed, possibly a consequence of the fact that in

protein lipid overlay assays the phosphoinositides are not embedded in a lipid membrane, and therefore the headgroup posititions of the phosphorylated inositols are neither defined, nor aligned, which may alter binding specificity. In agreement with a previous study (Soykan et al., 2014), the major Cb-isoform in the mammalian brain, SH3-CbII, which forms an autoinhibited conformation in which the SH3 domain interacts with the DH/PH tandem-domain, does not bind to any phosphoinositides. In the presence of both, TC10 (WT or the KR/GS mutant) and Cb, the SH3-CbII isoform shows altered binding capacities for certain phoshoinositides. (B) Relative phosphoinositide binding capacities of proteins, as indicated, determined by measuring the intensity of the chemiluminescence. The data represent means ± SEM of n=3 measurements.

## FIGURE S4

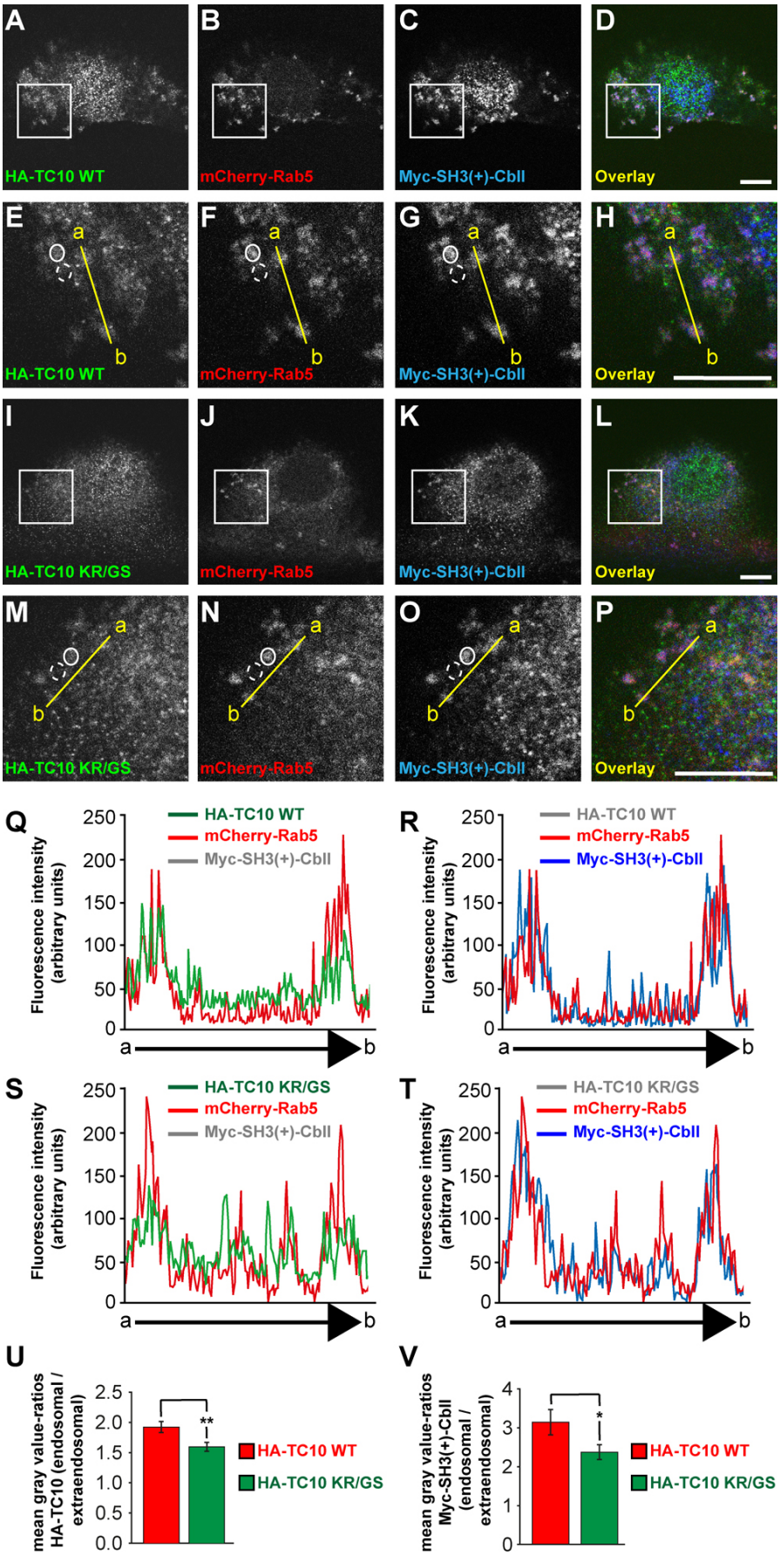

**Fig. S4. The KR/GS mutation affects the localization of Myc-SH3(+)-CbII/HA-TC10 complexes at mCherry-Rab5-labeled endosomes.**

(A-P) Exemplary confocal images of NIH-3T3 cells coexpressing HA-TC10 WT (A-H) or the HA-TC10 KR/GS mutant (I-P) together with Myc-SH3(+)-CbII and mCherry-Rab5, as indicated. (E-H and M-P) Magnifications of the boxed areas in A-D and I-L, respectively. Note the enriched immunoreactive signal of HA-TC10 WT (E; closed circle) and Myc-SH3(+)CbII (G; closed circle) in mCherry-Rab5-positive endosomes (F; closed circle), as compared to the signal in extraendosomal areas (dashed circles in E-G). In contrast, the endosomal accumulation of both, the HA-TC10 KR/GS mutant (M) and Myc-SH3(+)-CbII (O) was reduced, but not completely diminished in cells coexpressing these two proteins together with mCherry-Rab5 (M-O). Scale bars: 10 µm. (Q, S) Fluorescence intensity scans over the yellow lines in *E-H and M-P* [E: HA-TC10 WT, green; M: HA-TC10 KR/GS, green; F, N: mCherry-Rab5, red; Myc-SH3(+)-CbII in grey indicates that its corresponding fluorescence intensity scan is not shown], respectively. The line plots indicate accumulation of HA-TC10 WT (Q) and strongly reduced accumulation of the HA-TC10 KR/GS mutant (S) in mCherry-Rab5-positive endosomes. (R, T) Fluorescence intensity scans over the yellow lines in *E-H and M-P* [G: Myc-SH3(+)-CbII together with HA-TC10 WT, green; O: Myc-SH3(+)-CbII together with HA-TC10 KR/GS, green; F, N: mCherry-Rab5, red; HA-TC10 (WT or KR/GS) in grey indicates that the corresponding fluorescence intensity scan are not shown], respectively. The line plots indicate clear endosomal accumulation of Myc-SH3(+)-CbII in HA-TC10 WT coexpressing cells (R). The endosomal accumulation of Myc-SH3(+)-CbII in cells coexpressing the HA-TC10 KR/GS mutant is reduced, as compared to the extraendosomal signal in R and T. (U, V) For statistical comparison, the following ratios were calculated: (U) mean gray values of endosomal HA-TC10 / mean gray values of extraendosomal HA-TC10 [WT (red) or the KR/GS mutant (green)] and (V) mean gray values of endosomal Myc-SH3(+)-CbII / mean gray values of extraendosomal Myc-SH3(+)-CbII [in HA-TC10 WT (red) or HA-TC10 KR/GS expressing cells (green)]. Endosomal (closed circles) and extraendosomal (dashed circles) areas were preselected as exemplary indicated by the closed and dashed circles in *E* and *M*, respectively. For each cell, the mean gray values of at least 10 endosomal and 10 extraendosomal areas were calculated. The data represent means ± SEM (*$P$ < 0.05, **$P$ < 0.01; unpaired, two-tailed Student's t-test) of N=3 independent experiments and n=20 cells per condition.

## FIGURE S5

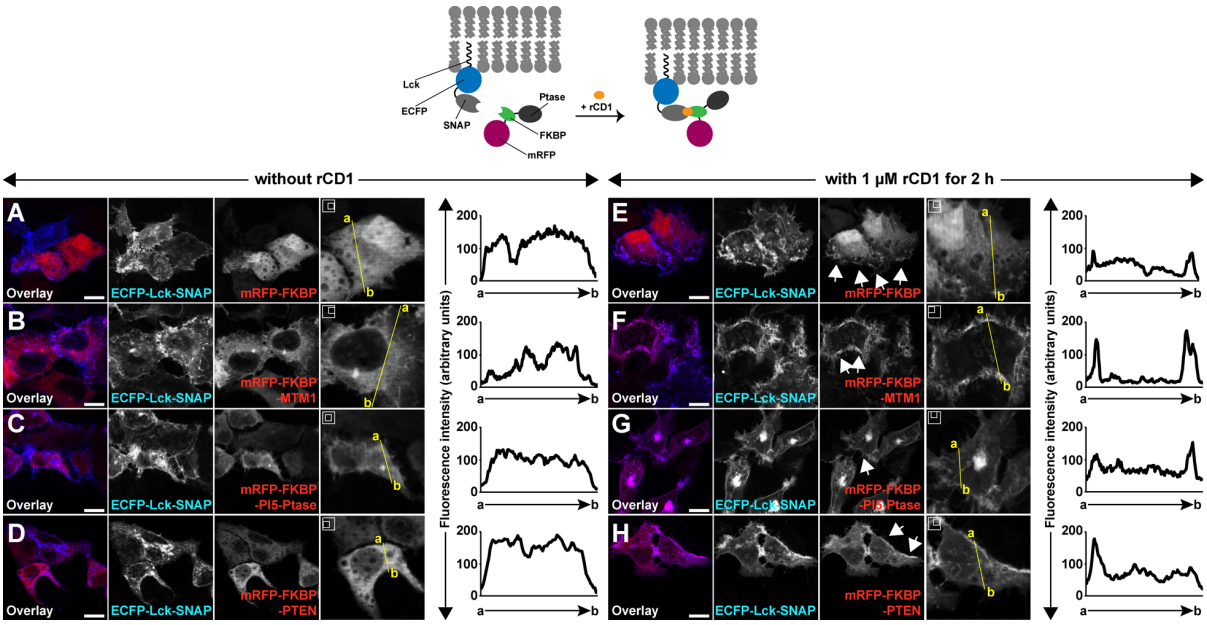


**Fig. S5. rCD1-based recruitment of FKBP-constructs to the plasma membrane.** Top: Schematic representation of the rCD1-based dimerization system for fast and efficient recruitment of proteins to the plasma membane. (A-H) Representative images of Flp-In T-Rex-EGFP-gephyrin HEK 293 cells cotransfected in their uninduced state (see *Materials and Methods*) with the plasma membrane anchor ECFP-Lck-SNAP (blue) and the different mRFP-FKBP constructs (red), as indicated. At 16 h post-transfection, the medium was replaced for 2h by serum-free DMEM (41966-029; Gibco) in the absence of rCD1 (A-D) or in the presence of 1 µM rCD1 (E-H). Note the cytosolic distribution of the mRFP-FKBP constructs in the absence of rCD1 (red channels in A-D). In contrast, a 2 h-treatment with 1 µM rCD1 efficiently induced translocation of the different mRFP-FKBP constructs to the plasma membrane (as indicated by arrows in E-H). Scale bars: 10 µm. Right panels in A-H: Magnifications of the corresponding channels of the mRFP-FKBP constructs as indicated in the rectangles shown in the upper left corners. Line-plots: Fluorescence intensity scans over the yellow lines of the corresponding images to their left, illustrating cytosolic distribution of the mRFP-FKBP constructs in the absence of rCD1 (A-D) and plasma membrane recruitment due to their interaction with ECFP-Lck-SNAP in the presence of 1 µM rCD1 (E-H).

**FIGURE S6**

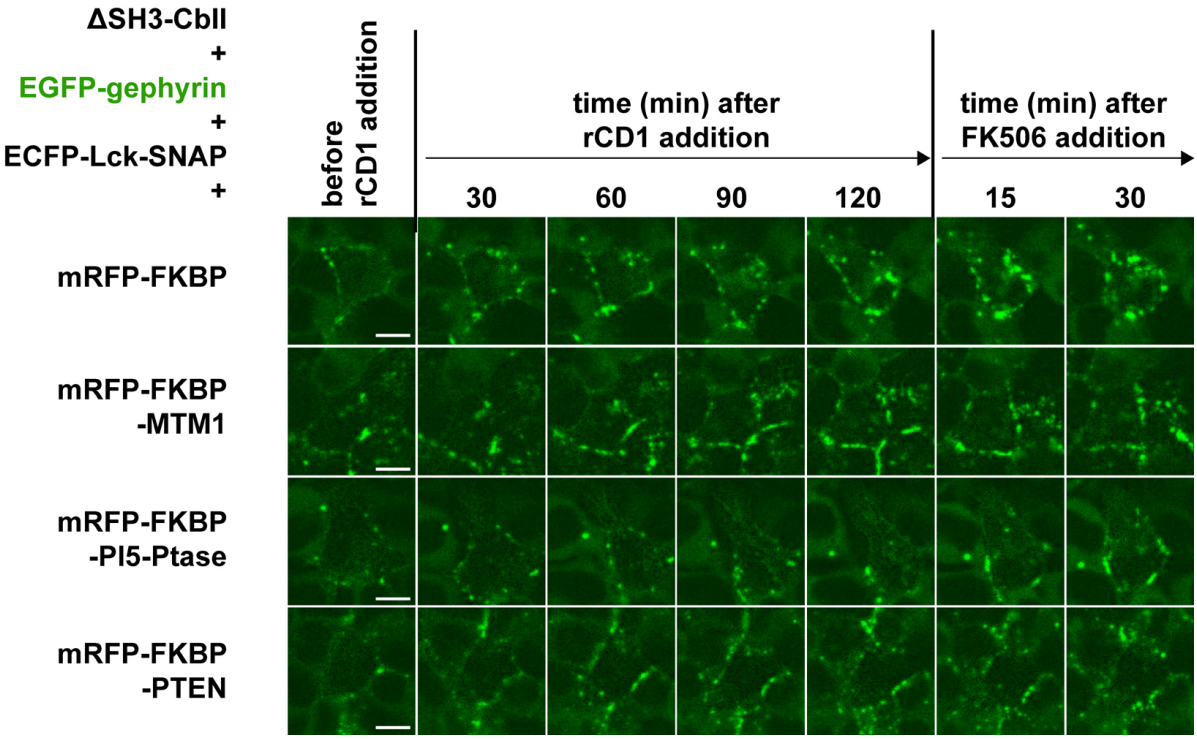


**Fig. S6. Corresponding EGFP-gephyrin channels of the time-lapse confocal fluorescence images of Flp-In T-Rex-EGFP-gephyrin shown in Fig. 6**. Cells were transfected and treated as indicated in the main text of the manuscript and in the legend to Fig. 6.

## FIGURE S7

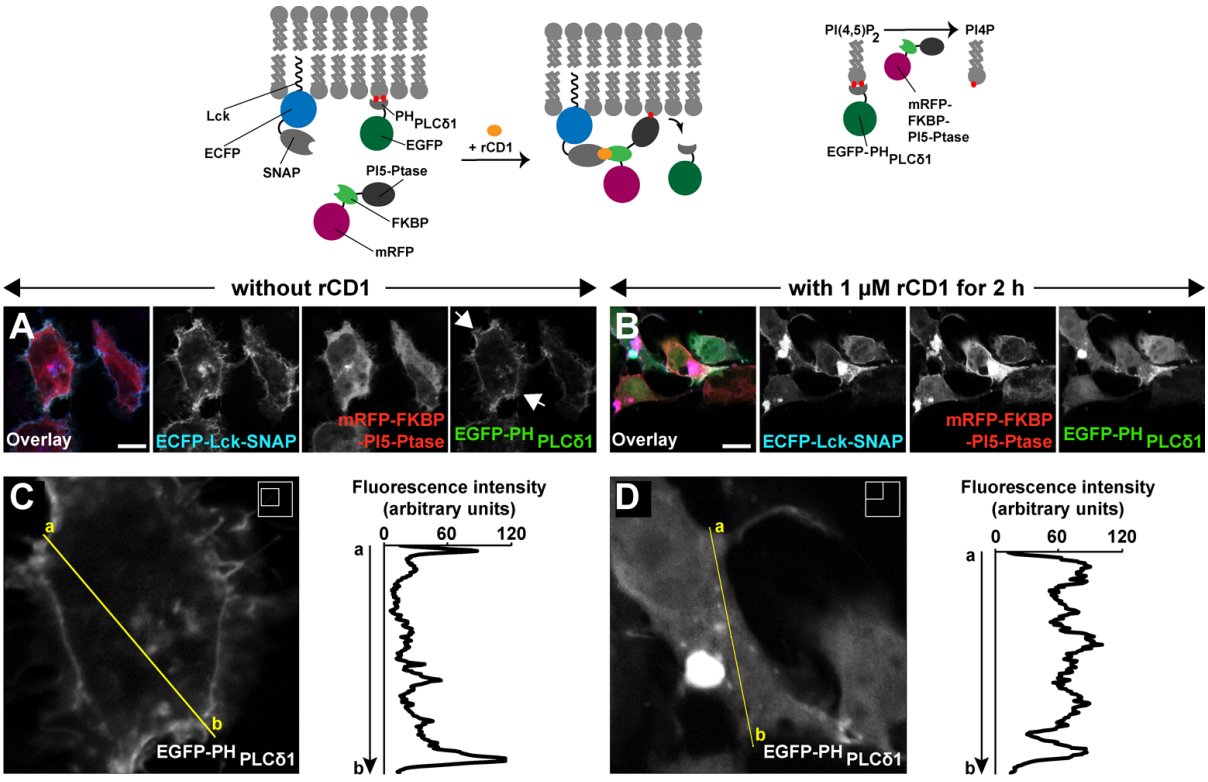


**Fig. S7. rDC1-dependent plasma membrane recruitment of mRFP-FKBP-PI5-Ptase efficiently depletes PI(4,5)$P_2$.** Top: Schematic representation of the rCD1-based recruitment of mRFP-FKBP-PI5-Ptase to the plasma membrane and the subsequent redistribution of EGFP-$PH_{PLC\delta1}$, a PI(4,5)$P_2$-specific probe. The rCD1-based dimerization of the membrane anchor ECFP-Lck-SNAP with mRFP-FKBP-PI5-Ptase leads to the conversion of PI(4,5)$P_2$ to PI4P. Thus, the EGFP-$PH_{PLC\delta1}$ probe cannot be anchored to the plasma membrane any more and redistributes into the cytosol. (A, B) Representative images of Flp-In T-Rex-EGFP-gephyrin HEK 293 cells cotransfected in their uninduced state (see *Materials and Methods*) with the plasma membrane anchor ECFP-Lck-SNAP (blue), mRFP-FKBP-PI5-Ptase (red) and EGFP-$PH_{PLC\delta1}$ (green), as indicated. At 16 h post-transfection, the medium was replaced for 2h by serum-free DMEM (41966-029; Gibco) in the absence of rCD1 (A) or in the presence of 1 µM rCD1 (B). Note the cytosolic distribution of mRFP-FKBP-PI5-Ptase (red) in the absence of rCD1 (A). In contrast, EGFP-$PH_{PLC\delta1}$ is mostly localized at the plasma mebrane (indicated by arrows) due to the accumulation of PI(4,5)$P_2$ at that compartment. (B) A 2 h-treatment with 1 µM rCD1 efficiently induced translocation of mRFP-FKB-PI5-Ptase to the plasma membrane and the subsequent redistribution of

EGFP-$PH_{PLC\delta1}$ into the cytosol, due to the depletion of $PI(4,5)P_2$. (C, D) Magnifications of the corresponding channels of EGFP-$PH_{PLC\delta1}$ in A and B, as indicated in the rectangles shown in the upper right corners. Line-plots: Fluorescence intensity scans over the yellow lines of the corresponding images to their left, illustrating plasma membrane localization of EGFP-$PH_{PLC\delta1}$ in the absence of rCD1 (C) and its cytosolic redistribution in the presence of 1 μM rCD1 (D).